Effect of axial load on flexural behaviour of cyclically loaded RC columns

F. T. K. Au[†] and Z. Z. Bai[‡]

*Department of Civil Engineering, The University of Hong Kong, Pokfulam Road,
Hong Kong, P.R. China*

Abstract. The flexural behaviour of symmetrically reinforced concrete (RC) columns cast of normal- and high-strength concrete under both monotonic and cyclic loading is studied based on an analytical procedure, which employs the actual stress-strain curves and takes into account the stress-path dependence of concrete and steel reinforcement. The analysis is particularly extended into the post-peak stage with large inelastic deformation at various applied axial load level. The effect of axial load on their complete flexural behaviour is then identified based on the results obtained. The axial load is found to have fairly large effect on the flexural behaviour of RC columns under both monotonic and cyclic loading. Such effects are discussed through examination of various aspects including the moment-curvature relationship, moment capacity, flexural ductility, variation of neutral axis depth and steel stress.

Keywords: axial load; flexural ductility; moment capacity; moment-curvature relationship; monotonic and cyclic loading; reinforced concrete columns.

1. Introduction

Hinging may appear in reinforced concrete (RC) columns under seismic type of loading. To evaluate the structural response under such conditions, knowledge of the complete flexural behaviour into the post-peak stage with large inelastic deformation is essential, especially when high-strength concrete (ACI Committee 363, 1992) that is inherently more brittle than normal-strength concrete has been increasingly used.

Numerous experiments on RC columns have been carried out in the past few decades. Sheikh and Yeh (1990) tested 15 normal-strength RC columns loaded monotonically with large inelastic deformations under constant axial load to investigate the behaviour of column sections confined by rectilinear ties. Azizinamini, *et al.* (1992) tested 12 full-scale columns subjected to constant axial load under cyclic loading to evaluate simplification of some of the detailing requirements. Later Azizinamini, *et al.* (1994) conducted experiments on 9 two-third scale high-strength concrete columns subjected to constant axial load and cyclic lateral loads to study flexural strength and ductility of high-strength RC columns. They found that the ACI 319-89 code provisions might overestimate their flexural capacities. Sakai and Sheikh (1989) provided a review on the subject of confinement on behaviour of normal-strength RC columns. Ho and Pam (2003) proposed some guidelines for the

---

design of low-axially loaded high-strength RC columns based on their experimental results. Hwang and Yun (2004) examined the flexural behaviour of 8 one-third scale high-strength concrete columns subjected to constant axial load and found that ACI 318-02 gave conservative estimates of nominal moment capacities of the tested specimens.

Various researchers have investigated the full-range flexural behaviour of RC beams, a case similar to RC columns but without axial loading. Carreira and Chu (1986) presented a general non-linear method to compute the moment-curvature relationship of RC beams. A numerical method for the full-range moment-curvature analysis of RC beams under monotonic or cyclic loading, which takes into account the non-linear stress-strain relationship and stress-path dependence of the constitutive materials, has been developed and applied to rectangular beams (Pam, *et al.* 2001, Kwan, *et al.* 2004, Au, *et al.* 2005, Bai, *et al.*) and flanged beams (Au and Kwan 2004, Kwan and Au 2004). Soroushian, *et al.* (1991) conducted a study on the effects of the design variable of RC columns based on a layer-model in which the strains at layers were obtained from curvature and the axial strain values at plastic centroid assuming a linear distribution of strain across section.

This paper describes an analytical study of the complete flexural behaviour of symmetrical RC columns cast of normal- and high-strength concrete under both monotonic and cyclic loading in the form of bending moment. Analysis is extended into the post-peak stage with large inelastic deformation. The investigation employs the actual stress-strain curves and takes into account the stress-path dependence of concrete and steel reinforcement. Constant axial load is applied at the geometric centre of sections at the beginning when the curvature or moment is zero. In particular, the effects of axial load are evaluated.

2. Stress-strain relationship of unconfined and confined concrete

For convenience, compressive stresses and strains of concrete are taken as positive while those in tension are negative. In the study, the unified compression stress-strain model for confined and unconfined concrete developed by Attard and Setunge (1996) and Attard and Stewart (1998), which has been shown to be applicable to a broad range of *in situ* concrete strength from 20 to 130 MPa, is employed. The main parameters used to establish this stress-strain model are the peak stress f_o and the corresponding strain ε_o, and two dimensionless coefficients A and B, which are dependent on the concrete grade and the confining stress. The relationship between the concrete stress σ_c and concrete strain ε_c is

$$\sigma_c/f_o = \frac{A(\varepsilon_c/\varepsilon_o)+B(\varepsilon_c/\varepsilon_o)^2}{1+(A-2)(\varepsilon_c/\varepsilon_o)+(B+1)(\varepsilon_c/\varepsilon_o)^2} \tag{1}$$

Taking into account confinement effect, the peak stress f_o and the corresponding strain ε_o are

$$f_o = f_{co}\left[1+\frac{f_r}{0.56\sqrt{f_{co}}}\right]^k \tag{2}$$

$$\varepsilon_o = \left[\frac{4.11(f_{co})^{0.75}}{E_c}\right]\left[1+(17.0-0.06f_{co})\frac{f_r}{f_{co}}\right] \tag{3}$$

where f_{co} is the peak stress under unconfined conditions, f_r is the confining stress, E_c is the initial

Young's modulus, and $k = 1.25(1+0.062f_r/f_{co})(f_{co})^{-0.21}$. Note that all stresses and moduli have the unit MPa. The peak stress f_{co} is actually the *in situ* uniaxial compressive strength of concrete, which may be determined from the standard cube or cylinder strengths using appropriate conversion factors.

Two sets of the coefficients A and B are required, with one for the ascending branch and another for the descending branch of the curve. For the ascending branch where $\varepsilon \leq \varepsilon_o$,

$$A = \frac{E_c \varepsilon_o}{f_o} \tag{4a}$$

$$B = \frac{(A-1)^2}{0.55} - 1 \tag{4b}$$

For the descending branch where $\varepsilon > \varepsilon_o$,

$$A = \left(\frac{\varepsilon_j - \varepsilon_i}{\varepsilon_o}\right)\left[\frac{\varepsilon_j f_i}{\varepsilon_i(f_o - f_i)} - \frac{4\varepsilon_i f_j}{\varepsilon_j(f_o - f_j)}\right] \tag{5a}$$

$$B = (\varepsilon_i - \varepsilon_j)\left[\frac{f_i}{\varepsilon_i(f_o - f_i)} - \frac{4f_j}{\varepsilon_j(f_o - f_j)}\right] \tag{5b}$$

where ε_i is the strain at the inflection point on the descending branch of the stress-strain curve, $\varepsilon_j = \varepsilon_i + (\varepsilon_i - \varepsilon_o)$, and f_i and f_j are stresses corresponding to ε_i and ε_j respectively. The values of ε_i, f_i and f_j have been obtained by analyzing available experimental data, which yields

$$\varepsilon_i = \varepsilon_o\left[2 + \frac{2.5 - 0.3\ln(f_{co}) - 2}{1 + 1.12(f_r/f_{co})^{0.20}}\right] \tag{6a}$$

$$f_i = f_o\left[1 + \frac{1.41 - 0.17\ln(f_{co}) - 1}{1 + 5.06(f_r/f_{co})^{0.57}}\right] \tag{6b}$$

$$f_j = f_o\left[1 + \frac{1.45 - 0.25\ln(f_{co}) - 1}{1 + 6.35(f_r/f_{co})^{0.62}}\right] \tag{6c}$$

(a) Unconfined concrete of various grade   (b) Confined concrete with f_{co} = 60MPa
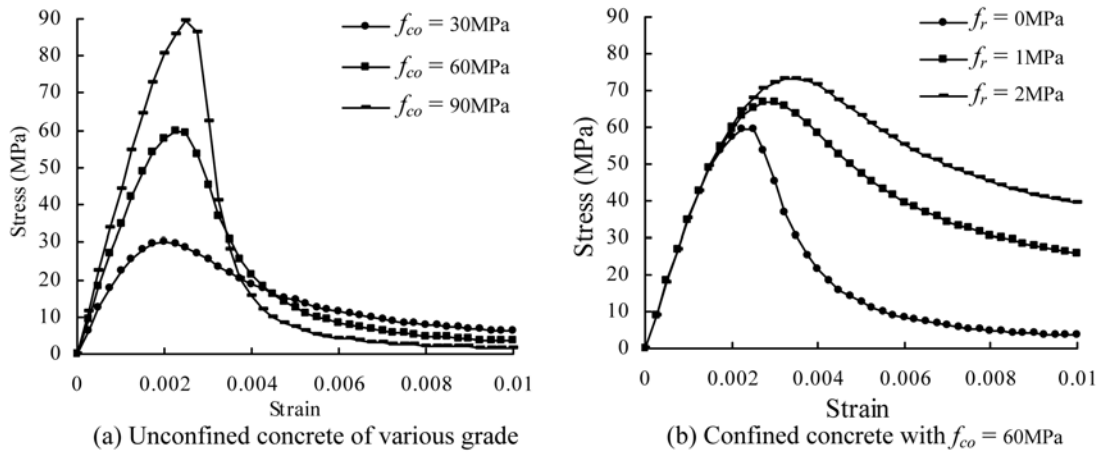
Fig. 1 Stress-strain curves of concrete in compression

Fig. 1(a) shows some typical stress-strain curves of unconfined concrete for *in situ* concrete strength from 30 to 90 MPa, while Fig. 1(b) shows those of confined concrete with f_{co} equal to 60 MPa and f_r ranging from 0 to 2 MPa.

The tensile stress-strain curve of concrete before cracking follows a straight line with slope E_c. For the post-cracking behaviour, the model proposed by Guo and Zhang (1987) is adopted, namely

$$\frac{\sigma_c}{f_t} = \frac{\varepsilon_c/\varepsilon_t}{\alpha(\varepsilon_c/\varepsilon_t - 1)^{1.7} + \varepsilon_c/\varepsilon_t} \qquad (7)$$

where f_t is the tensile strength, ε_t is the tensile strain at tensile strength, and α is a parameter dependent on the concrete grade.

Fig. 2(a) shows a typical path 0-1-2-2'-3-4 for idealized cyclic response of concrete in compression. After loading along the envelope to point 1 (ε_{un}^c, σ_{un}^c), unloading goes towards point 2 (ε_{pc}, 0), along the straight initial unloading region 1-2, followed by a zero stiffness region 2-2'. According to Elmorsi, *et al.* (1998), the slope E_{un} of the initial unloading path 1-2 can be given in terms of the unloading strain ε_{un}^c and the strain at peak compressive stress ε_{co} as

$$\frac{E_{un}}{E_c} = 1 \quad \text{for} \quad \frac{\varepsilon_{un}^c}{\varepsilon_{co}} \le 1 \qquad (8a)$$

$$\frac{E_{un}}{E_c} = 1 - 0.3\left(\frac{\varepsilon_{un}^c}{\varepsilon_{co}} - 1\right) \ge 0.25 \quad \text{for} \quad \frac{\varepsilon_{un}^c}{\varepsilon_{co}} > 1 \qquad (8b)$$

If reloading takes place in the initial unloading region 1-2, it retraces the same unloading path until it reaches the envelope. However reloading from a point on the zero stress region follows a different path, for example path 2'-g-3. Paths 2'-3 and 1-2 intersect at the common point g (ε_{cp}, σ_{cp}) that is assumed to be the one on the initial unloading curve with $\sigma_{cp} = 0.7\sigma_{un}^c$ and therefore the stiffness E_{re} on reloading can be worked out accordingly. During unloading and reloading, the stress σ_c is related to the strain ε_c by

(a) Cyclic response of concrete in compression

(b) Cyclic response of concrete in tension and interaction between compression and tension
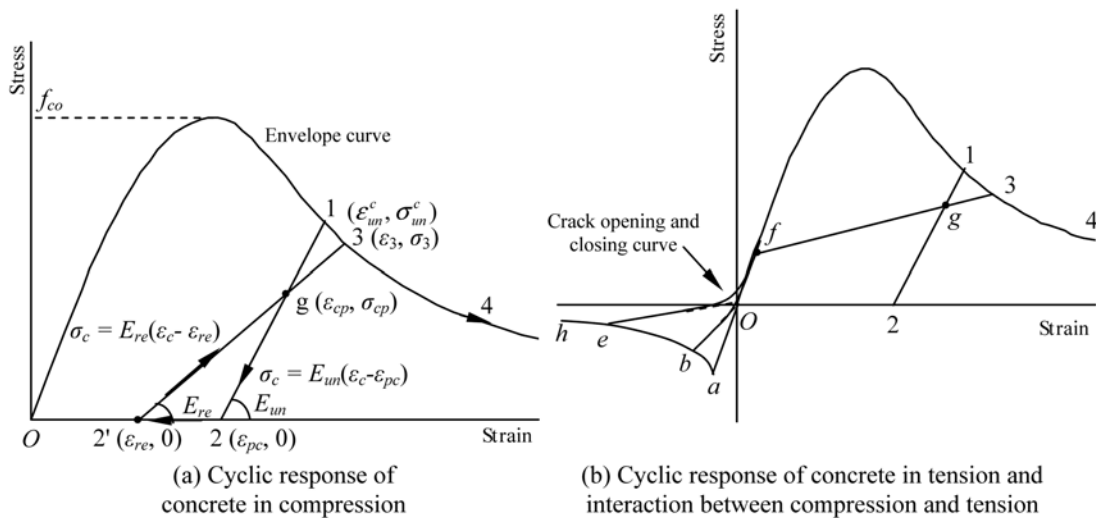
Fig. 2 Stress-strain relationship of concrete with stress path dependence

$$\sigma_c = E_{un}(\varepsilon_c - \varepsilon_{pc}) \text{ for } \varepsilon_{pc} \leq \varepsilon_c \leq \varepsilon_{un}^c \qquad \text{(initial unloading region)} \qquad (9a)$$

$$\sigma_c = 0 \text{ for } \varepsilon_{re} < \varepsilon_c < \varepsilon_{pc} \qquad \text{(zero stiffness region)} \qquad (9b)$$

$$\sigma_c = E_{re}(\varepsilon_c - \varepsilon_{re}) \text{ for } \varepsilon_{re} \leq \varepsilon_c \leq \varepsilon_3 \qquad \text{(reloading)} \qquad (9c)$$

If unloading from the compression region goes beyond the origin O, it follows the straight line O-a until the tensile strength is reached, and then the tension softening curve a-b in Fig. 2(b). If the load is again reversed from point b (ε_{un}^t, σ_{un}^t), the crack opening and closing curve b-f and the straight line f-g-3 are followed until the envelope curve in compression is reached again, where f (ε_{fp}, σ_{fp}) is the common point on the compressive envelope curve with stress $0.1f_{co}$. The curve used to describe the crack opening and closing effect was originally developed by Menegotto and Pinto (1973) for reinforcing steel but its properties have made it suitable for the current application. The equation of this curve is expressed as

$$\sigma^* = b\varepsilon^* + \frac{(1-b)\varepsilon^*}{(1+\varepsilon^{*R})^{1/R}} \qquad (10)$$

where $b = \dfrac{\sigma_{un}^t / \varepsilon_{un}^t}{\sigma_{fp} / \varepsilon_{fp}}$, $R = R_o \dfrac{a_1 \varepsilon_{un}^t}{a_2 + \varepsilon_{un}^t}$, $\sigma^* = \dfrac{(\sigma_{fp} - \sigma_c)}{\sigma_{fp}}$ and $\varepsilon^* = \dfrac{(\varepsilon_{fp} - \varepsilon_c)}{\varepsilon_{fp}}$. The constants R_o, a_1 and a_2 are assumed to be 20, 18.5 and 0.0015, respectively.

3. Stress-strain relationship of steel with stress-path dependence

   Sagging moments are taken to be positive. For convenience, the top and bottom steel bars are referred to as the compression and tension reinforcement regardless of the nature of stresses carried at a particular instant. The sign conventions adopted for steel are as follows: (a) compressive stress and strain in compression reinforcement are positive; and (b) tensile stress and strain in tension reinforcement are positive. Fig. 3 shows the bilinear model adopted, which comprises an initial
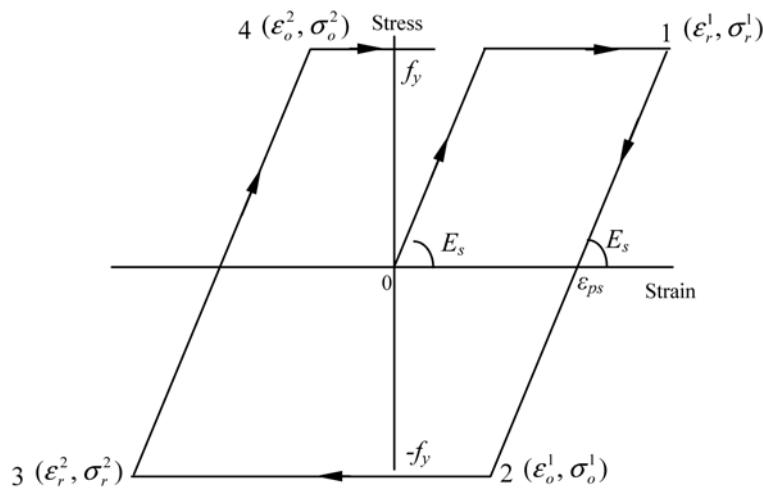

Fig. 3 Cyclic response of steel

elastic region and a yield plateau followed by the unloading paths. When the strain ε_s increases, the steel stress σ_s is given by

$$\sigma_s = E_s \varepsilon_s \text{ for } \varepsilon_s \leq f_y / E_s \text{ (at elastic stage)} \tag{11a}$$

$$\sigma_s = f_y \text{ for } \varepsilon_s > f_y / E_s \text{ (after yielding)} \tag{11b}$$

where E_s is Young's modulus and f_y is the yield stress. When strain reverses from a typical point 1 (ε_r^1, σ_r^1) on the yield plateau, it follows the inclined path 1-2 with slope E_s and then horizontal line 2-3 when it reaches yield stress in the opposite direction. A further strain reversal from point 3 then follows the inclined path 3-4 with slope E_s and then horizontal line 4-1. The stress-strain relationship along the inclined and horizontal paths are respectively given by

$$\sigma_s = E_s(\varepsilon_s - \varepsilon_{ps}) \text{ for inclined path} \tag{12a}$$

$$\sigma_s = f_y \text{ for positive horizontal path} \tag{12b}$$

$$\sigma_s = -f_y \text{ for negative horizontal path} \tag{12c}$$

where ε_{ps} is the residual strain for the inclined path. Bauschinger effect has not been taken into account.

4. Non-linear analysis

It is assumed that a constant resultant axial load is applied and maintained at the geometric centre of the column section before any bending moment is applied. Compressive axial loads are taken as positive. The usual assumption that plane sections remain plane and orthogonal after deformation is adopted. The average strain in steel is therefore equal to the average strain in concrete at the same level. Fig. 4(a) shows a section having a breadth b and a total depth h, with the tension reinforcement area A_{st} provided at a depth d and the compression reinforcement area A_{sc} provided at a depth d_1 from the top. Transverse links are provided so that the longitudinal steel bars are


(a) A rectangular section   (b) Strain distribution
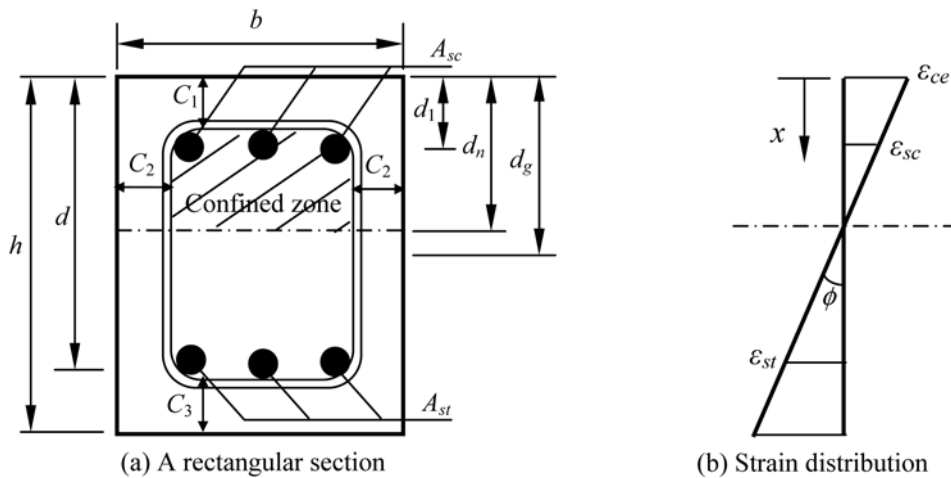
Fig. 4 A section subjected to combined axial load and bending moment

provided with top cover c_1, side cover c_2 and bottom cover c_3. It is assumed that the shaded rectangular area of concrete in compression is confined while the concrete elsewhere is unconfined. When the curvature of the section is increased to ϕ as shown in Fig. 4(b), the strain ε at a concrete fibre at a depth x from the extreme top fibre is given in terms of the neutral axis depth d_n as

$$\varepsilon = \phi(d_n - x) \tag{13}$$

The compressive strain ε_{ce} at the extreme concrete compression fibre, the compressive strain ε_{sc} in the compression reinforcement and the tensile strain ε_{st} in the tension reinforcement can be written respectively as

$$\varepsilon_{ce} = \phi \, d_n \tag{14a}$$

$$\varepsilon_{sc} = \phi \, (d_n - d_1) \tag{14b}$$

$$\varepsilon_{st} = \phi \, (d - d_n) \tag{14c}$$

The corresponding stresses σ_c, $\sigma_c{}'$, σ_{sc} and σ_{st} developed in the unconfined concrete, confined concrete, compression reinforcement and tension reinforcement respectively can then be evaluated from the respective stress-strain relationships of the materials taking into account stress path dependence.

The stresses developed in the section must satisfy the conditions of axial and moment equilibrium. The resisting axial load P can be obtained from axial equilibrium as

$$P = \int_0^h \sigma_c b \, dx + \int_{c_1}^{h-c_3} (\sigma_c{}' - \sigma_c)(b - 2c_2)dx + A_{sc}\sigma_{sc} - A_{st}\sigma_{st} \tag{15}$$

Similarly, the resisting moment M can be obtained from moment equilibrium as

$$M = \int_0^h \sigma_c b(d_g - x)dx + \int_{c_1}^{h-c_3} (\sigma_c{}' - \sigma_c)(b - 2c_2)(d_g - x)dx + A_{sc}\sigma_{sc}(d_g - d_1) + A_{st}\sigma_{st}(d - d_g) \tag{16}$$

where d_g is the depth to the section geometric centre. In the evaluation of integrals in Eqs. (15) and (16), Romberg integration (Gerald and Wheatley 1999), which can significantly improve the accuracy of the simple trapezoidal rule when the integrand is known at equi-spaced intervals, has been adopted. The axial equilibrium condition as shown in Eq. (15) can be used to determine the neutral axis depth d_n. Normally, given a specified curvature ϕ and a trial value of neutral axis depth d_n, the equilibrium condition is not satisfied immediately and there is an error in the axial force. Since the relationship between the axial force error and the neutral axis depth d_n is nonlinear, an iterative scheme is required to determine the correct value of d_n. The scheme adopted here is the modified linear interpolation method (Gerald and Wheatley 1999). Finally, the moment-curvature relationship can be obtained.

5. Results of analysis

5.1. Sections analyzed

The sections analyzed are rectangular in shape as shown in Fig. 4(a). A typical symmetrically RC

column section has a breadth $b = 300$ mm and total depth $h = 600$ mm, with the reinforcement provided at depths $d_1 = 50$ mm and $d = 550$ mm from the top respectively, and with cover $c_1 = c_2 = c_3 = 40$ mm. The steel reinforcement has a yield strength $f_y = 460$ MPa and Young's modulus $E_s = 200$ GPa. The *in situ* concrete compressive strength f_{co} ranges from 30 to 90 MPa to cover both normal- and high-strength concrete. The compression steel ratio $\rho_c = A_{sc}/bd$ and tension steel ratio $\rho_t = A_{st}/bd$ both vary from 1% to 4%. The confining stress has a fixed value of 1 MPa. In view of the length limitation, only some of the typical cases are included below for discussion.

5.2. Monotonic loading

Fig. 5 shows the effect of axial loading on the full-range moment-curvature curves for sections cast of normal- and high-strength concrete. Each family of curves follows nearly the same slope initially when the strain throughout the section is compressive. With further increase in curvature and hence cracking at the bottom, stiffness degradation with slope reduction is observed. Sections
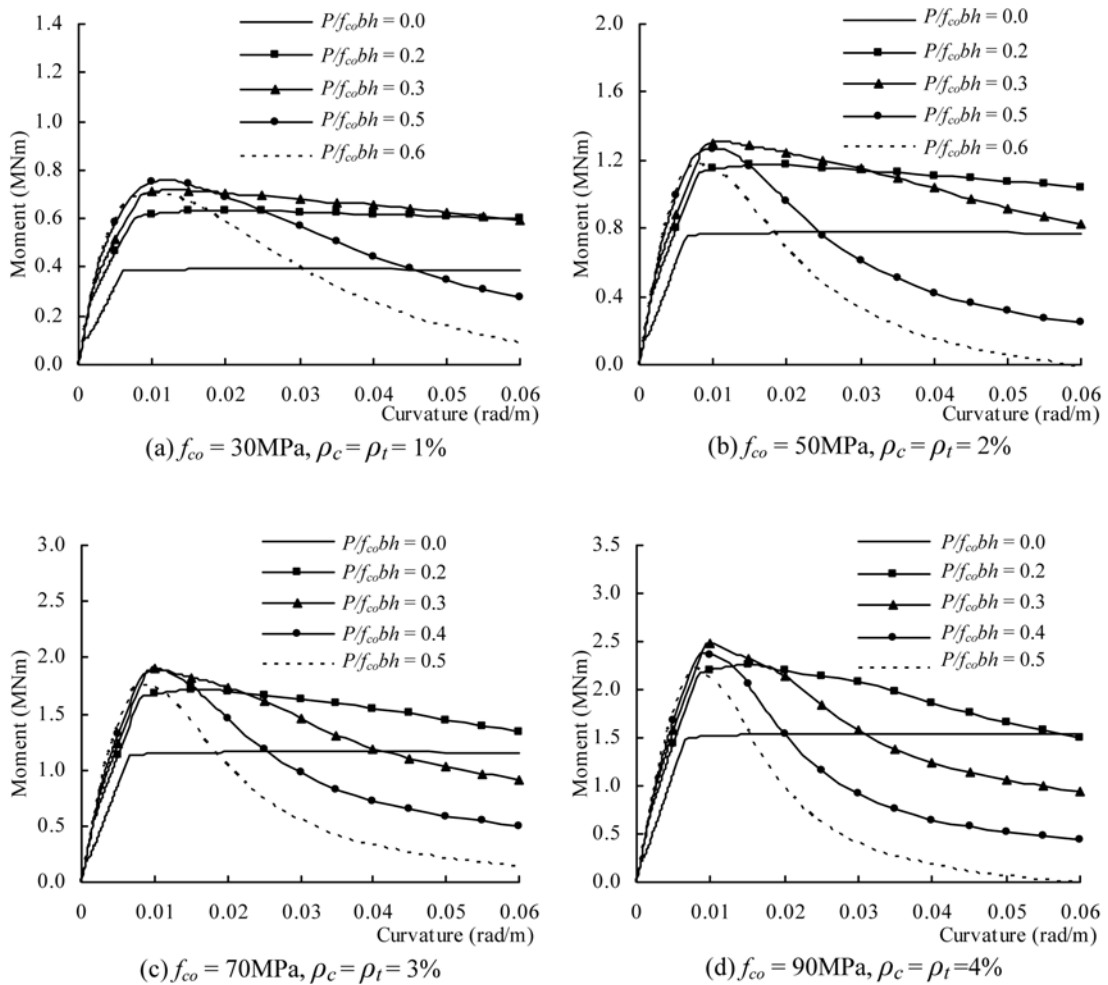
Fig. 5 Effect of axial load on complete moment-curvature curves
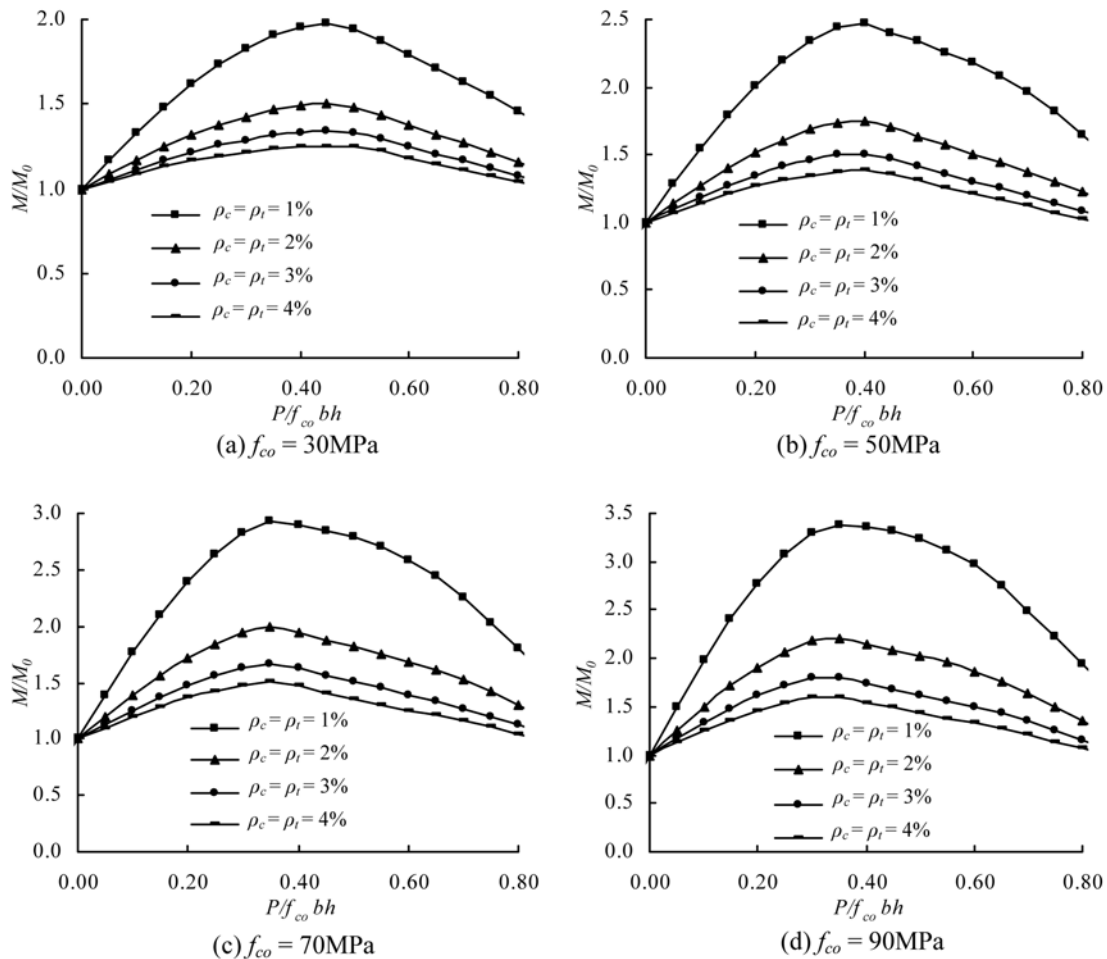
Fig. 6 Effect of axial load on moment capacity

under relatively low axial loading have cracks occurring at small curvatures, followed by a plateau in the moment-curvature curve around the peak moment. With the increase in axial load, the plateau gradually disappears and the curve becomes sharper around the peak moment indicating drastic reduction in ductility. This may be explained by the increasing reliance upon concrete compression with increasing axial loading.

The axial load level is an important parameter that determines not only the shape of moment-curvature curve but also the moment capacity and flexural ductility. Fig. 6 sums up the relationship between the moment capacity ratio M/M_0 and the axial load ratio $P/f_{co}bh$ for the sections, where M_0 is the moment capacity of the section without axial loading. The moment capacity tends to increase with compressive axial loading up to around $P/f_{co}bh = 0.4$ or 0.5, beyond which the moment capacity drops. The moment capacities of lightly reinforced sections are much more sensitive to the axial loading compared to those with heavier reinforcement.

The curvature ductility factor μ of a section can be evaluated from the moment-curvature curve in terms of the ultimate curvature ϕ_u and yield curvature ϕ_y as

(a) f_{co} = 30MPa

(b) f_{co} = 50MPa

(c) f_{co} = 70MPa

(d) f_{co} = 90MPa
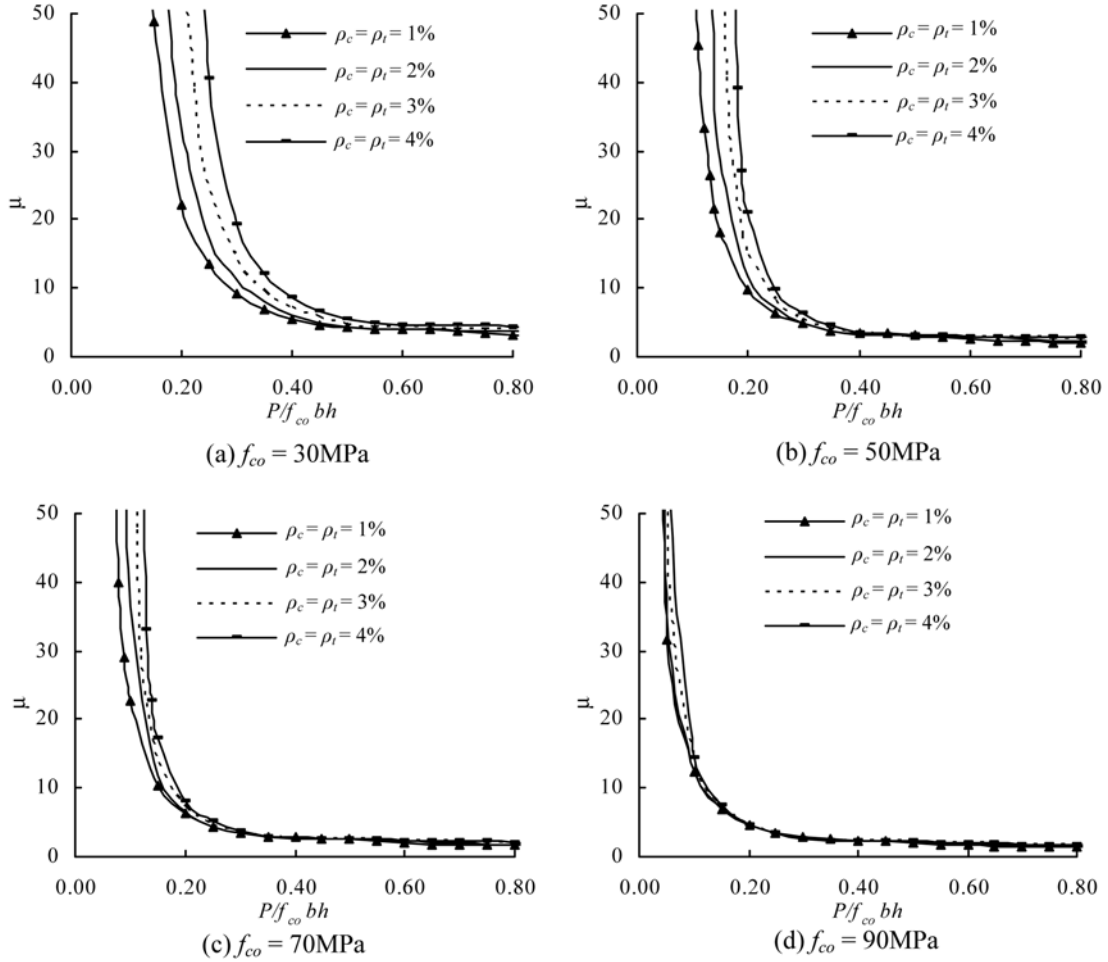
Fig. 7 Effect of axial load on curvature ductility factor

$$\mu = \phi_u / \phi_y \qquad\qquad (17)$$

The ultimate curvature ϕ_u is defined as the curvature of the section when its resisting moment has dropped to 80% of the peak moment after reaching the peak. The yield curvature ϕ_y is taken as that at the hypothetical yield point of an equivalent linearly elastic-perfectly plastic system with an elastic stiffness equal to the secant stiffness of the section at 75% of the peak moment and a yield moment equal to the peak moment. Fig. 7 shows the flexural ductility factor μ of the sections. With increasing axial loading and hence more reliance on concrete in compression, the flexural ductility factor always decreases. However under the same axial load ratio $P/f_{co}bh$, the flexural ductility factor increases with the reinforcement ratio as this reduces the reliance on concrete in compression. The effect of reinforcement ratio on flexural ductility is more significant for sections of normal-strength concrete while the effect is minimal when high-strength concrete is used.

Fig. 8 shows the variations of steel stresses for a section of *in situ* concrete strength 60 MPa, indicating different trends under different axial load levels. Except for very low axial load levels,

(a) Compression reinforcement

(b) Tension reinforcement
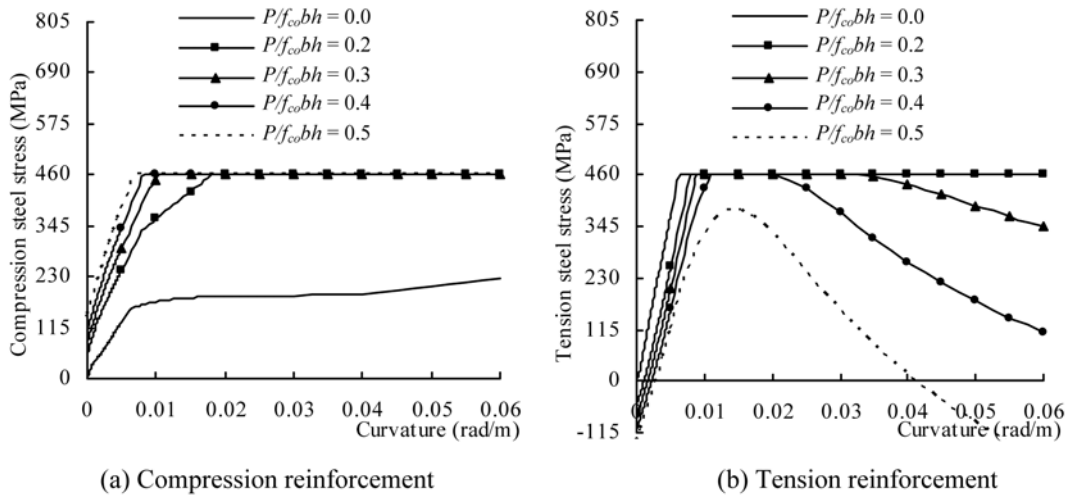
Fig. 8 Variation of steel stress of section under monotonic loading (*in situ* concrete strength = 60 MPa; $\rho_c = \rho_t = 2\%$)

(a) $\rho_c = \rho_t = 2\%$

(b) $\rho_c = \rho_t = 3\%$
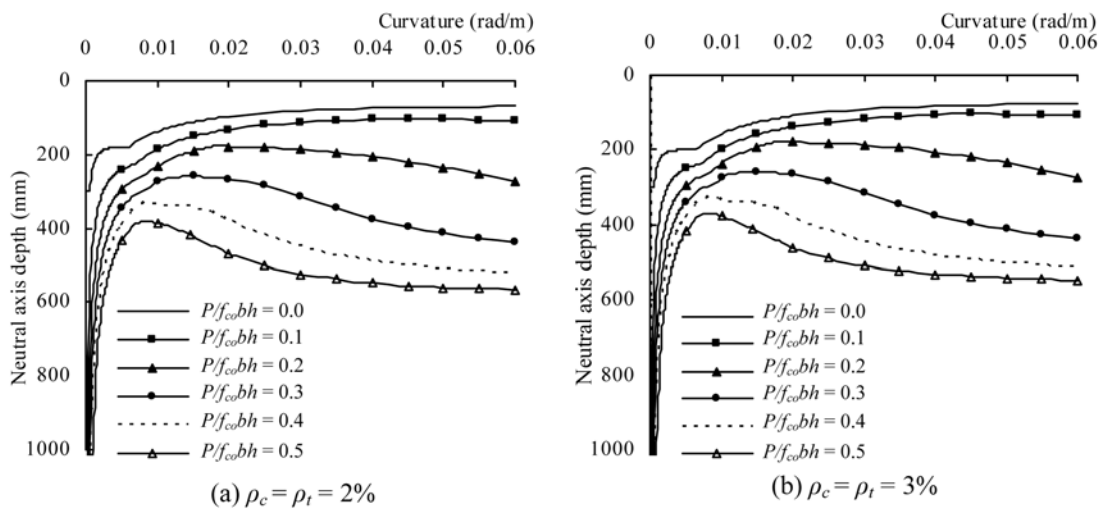
Fig. 9 Effect of axial load on neutral axis depth of sections under monotonic loading (*in situ* concrete strength = 60 MPa)

the compression reinforcement yields under loading and remains yielded. In most cases, the tension reinforcement yields with strain reversal and unloading at the post-peak stage. In the absence of axial loading or at very low axial loading, the tension reinforcement yields but does not unload. Under sufficiently high compressive axial loading (e.g. $P/f_{co}bh = 0.5$), the tension reinforcement does not yield at all.

The variation of neutral axis depth d_n of two sections under various axial loading as shown in Fig. 9 indicates that the variation depends on the axial load level. Except for the case without axial load, the neutral axis depth is theoretically infinite at infinitesimal curvature but it decreases rapidly as the curvature increases. When the axial loading is relatively low (i.e. $P/f_{co}bh \leq 0.1$), the neutral axis

depth keeps on decreasing with curvature. For medium to high axial load ratio $P/f_{co}bh$, the neutral axis depth increases again beyond a certain curvature at the post-peak stage giving rise to strain reversal at the tension steel. At the same curvature, the neutral axis depth is larger for higher compressive axial loads.

5.3. Cyclic loading

A typical reversed cycle of flexural loading consists of two half-cycles. In the first half-cycle, the curvature is increased from the origin (i.e. point o) to a maximum sagging value (i.e. point a) and then decreased to zero curvature (i.e. point b or b'). In the second half-cycle, it is loaded to a maximum hogging curvature (i.e. point c) and the curvature is then brought to zero (i.e. point d or d') again. The section may then be loaded to a larger sagging curvature (i.e. point e) or another cycle of loading may be carried out. For brevity in presentation, point b or d may be omitted. In view of the complexity of reversed cyclic loading, investigation is carried out separately on the first and second half-cycles. Provided that the imposed curvatures are big enough, the section bottom cracks during monotonic loading in sagging moment to point a. During the reversal from points a to c, the bottom crack closes while the section top cracks. In the reversal from points c to e, the top crack closes again while the bottom crack reopens. Crack opening and closure do affect the consequent properties of an RC column section. For simplicity, the curvature at crack opening or closure is approximately taken as that when the strain of corresponding concrete fibre becomes zero during its variation.

In the first half-cycle, the curvature is increased to point a (i.e. a_1, a_2, a_3, a_4, a_5 or a_6) and then decreased to a large hogging curvature at point c. The moment-curvature relationships of sections with *in situ* concrete strength 30 and 90 MPa are shown in Figs. 10 and 11 respectively with the location of bottom crack closure indicated. In these figures, both the moment-curvature curves under monotonic loading of sagging and hogging moments are shown in solid line for reference, while those for cyclic response from points a to c are shown in dash line. For cases of relatively low compressive axial loading (i.e. Figs. 10(a)-(c) and 11(a)-(c)) so that ductility remains very high, reversal from any large sagging curvature (i.e. a_1, a_2, a_3, a_4, a_5 or a_6) follows a straight line and then a horizontal line in the fourth quadrant, which reflects the unloading branch and yielding in the opposite direction shown in the stress-strain curve in Fig. 3. At a certain small hogging curvature, there is a sharp increase in flexural resistance round a well-defined point due to the closure of bottom cracks. Beyond the point of crack closure, the curve converges to the moment-curvature curve under monotonic loading of hogging moment. The ratio of moment at bottom crack closure to the peak hogging moment at monotonic loading is observed to decrease as the axial load increases. For cases of higher compressive axial loading (e.g. Figs. 10(d)-(e) and 11(d)-(e)) where ductility is slightly lower, the roughly straight line for unloading is followed by a transition curve in the fourth quadrant approaching the moment-curvature curve under monotonic loading of hogging moment. The behaviour of sections under even higher axial loading with even lower ductility (e.g. Figs. 10(f) and 11(f)) is similar except that the flexural resistance against hogging moment may deviate from that corresponding to the moment-curvature curve under monotonic loading of hogging moment. To sum up, the moment-curvature relationship of the first half-cycle depends mainly on the axial load level and the curvature at unloading (i.e. point a). However the above results show that the cyclic flexural behaviour is closely related to the ductility under monotonic loading of sagging moment but is not simply governed by clear-cut numerical values of axial load ratio $P/f_{co}bh$. Except for cases of
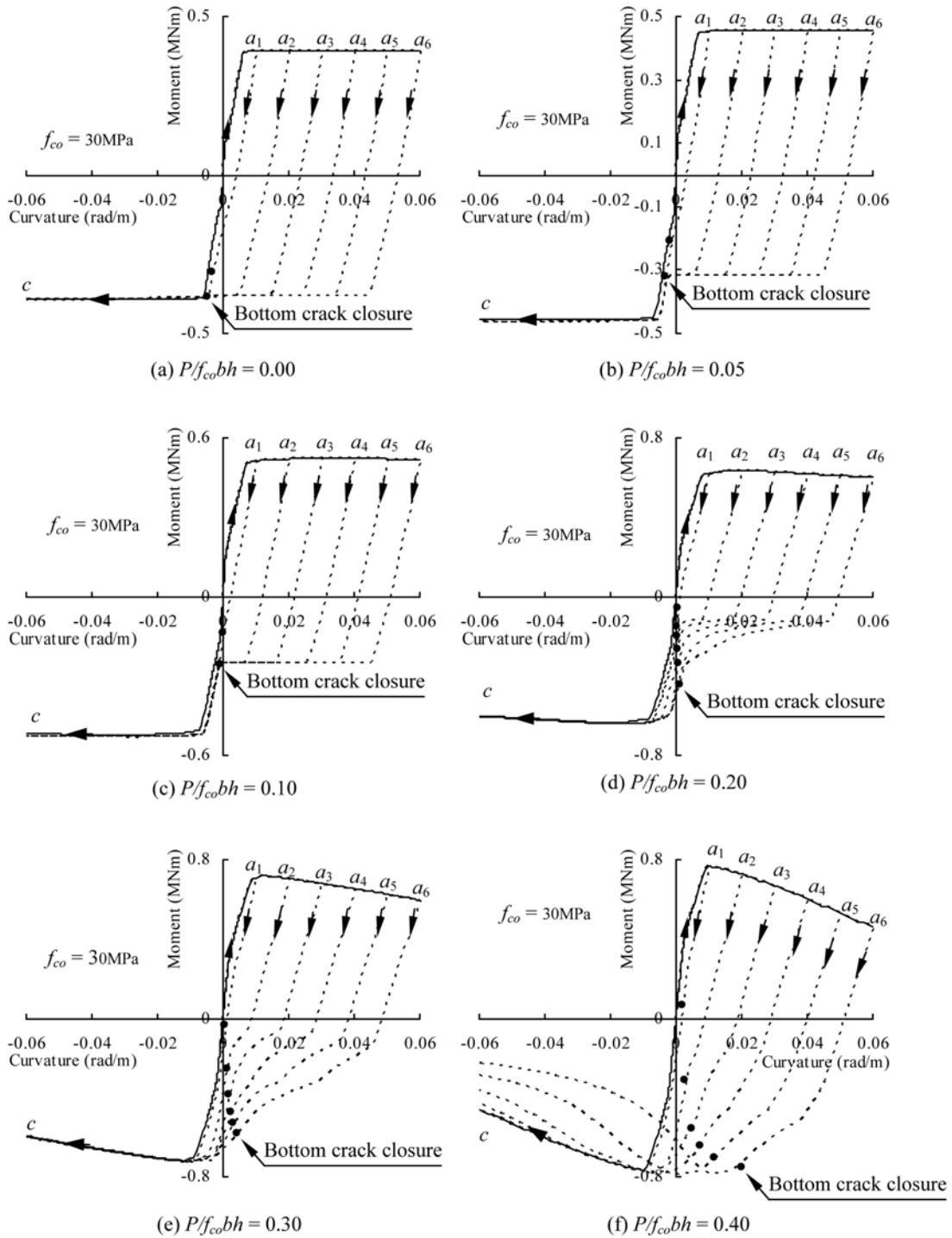
Fig. 10 Moment-curvature relationship of sections under cyclic loading (*in situ* concrete strength = 30 MPa; $\rho_c = \rho_t = 1\%$)

(a) $P/f_{co}bh = 0.00$

(b) $P/f_{co}bh = 0.05$

(c) $P/f_{co}bh = 0.10$

(d) $P/f_{co}bh = 0.15$

(e) $P/f_{co}bh = 0.17$

(f) $P/f_{co}bh = 0.20$
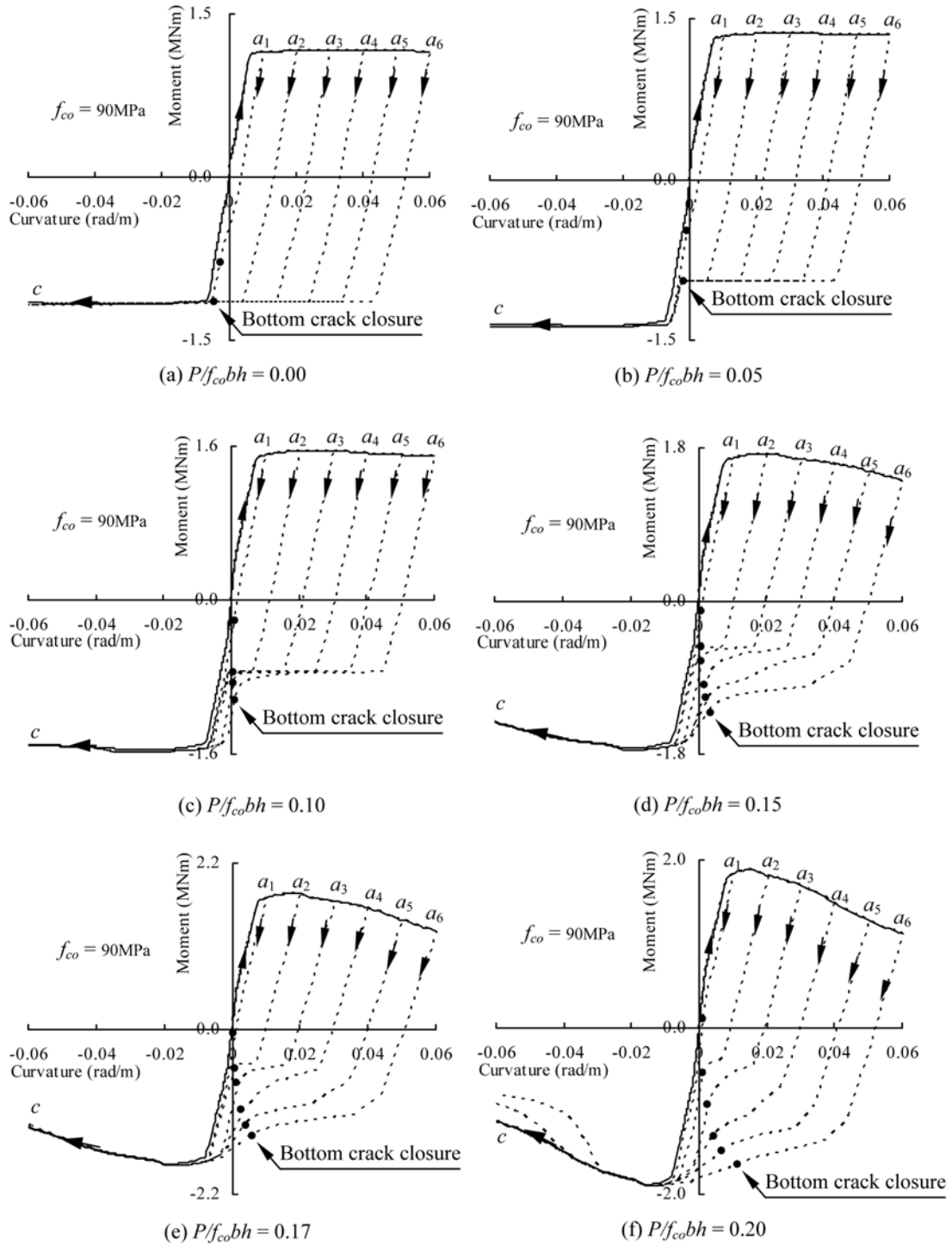
Fig. 11 Moment-curvature relationship of section under cyclic loading (*in situ* concrete strength = 90 MPa; $\rho_c = \rho_t = 3\%$)

(a) $P/f_{co}bh = 0.00$

(b) $P/f_{co}bh = 0.05$

(c) $P/f_{co}bh = 0.10$

(d) $P/f_{co}bh = 0.20$

(e) $P/f_{co}bh = 0.30$

(f) $P/f_{co}bh = 0.40$
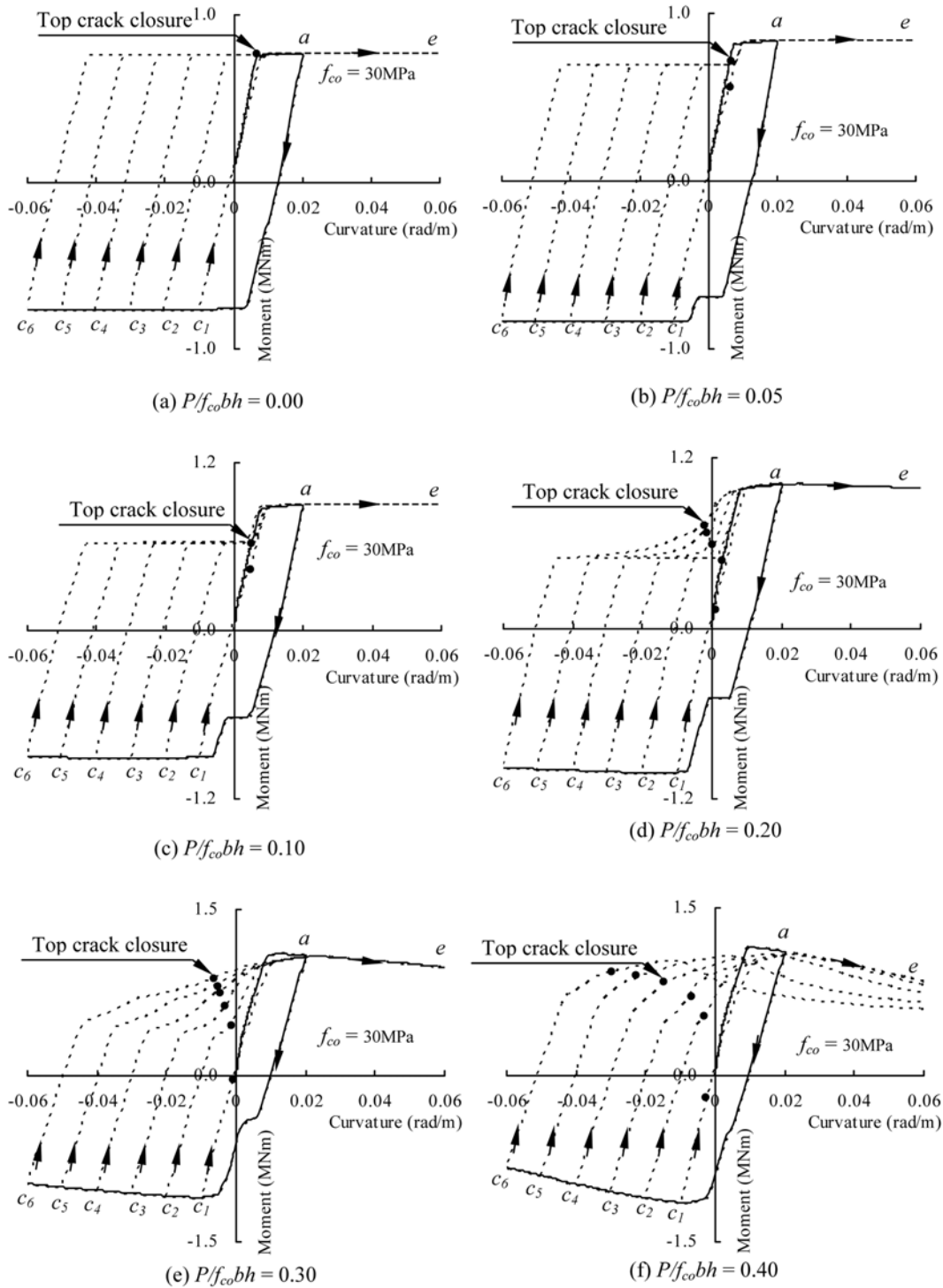
Fig. 12 Moment-curvature relationship of section under cyclic loading (*in situ* concrete strength = 30 MPa; $\rho_c = \rho_t = 2\%$)

(a) $P/f_{co}bh = 0.00$

(b) $P/f_{co}bh = 0.05$

(c) $P/f_{co}bh = 0.10$

(d) $P/f_{co}bh = 0.15$

(e) $P/f_{co}bh = 0.17$

(e) $P/f_{co}bh = 0.20$
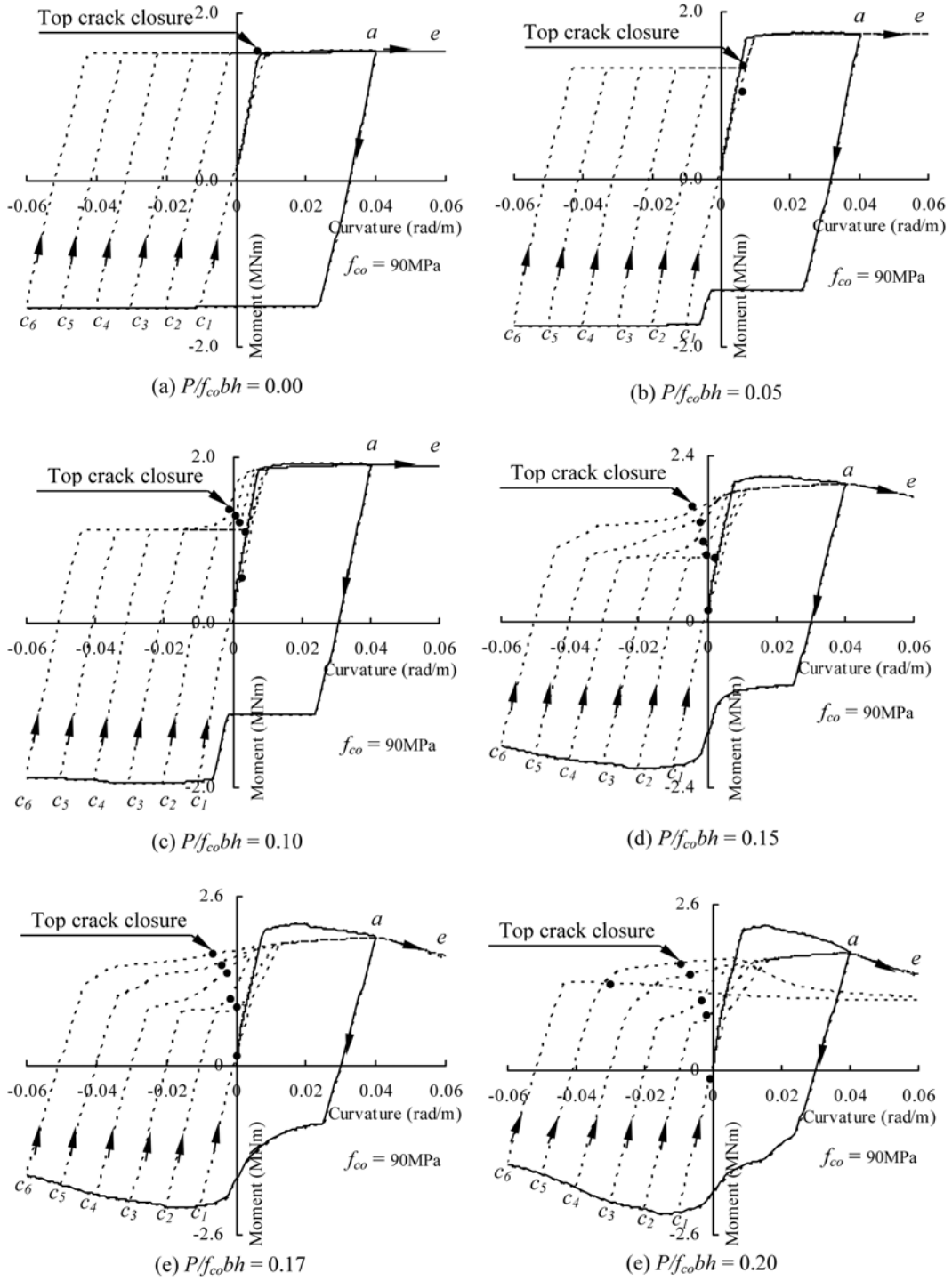
Fig. 13 Moment-curvature relationship of section under cyclic loading (*in situ* concrete strength = 90 MPa; $\rho_c = \rho_t = 4\%$)
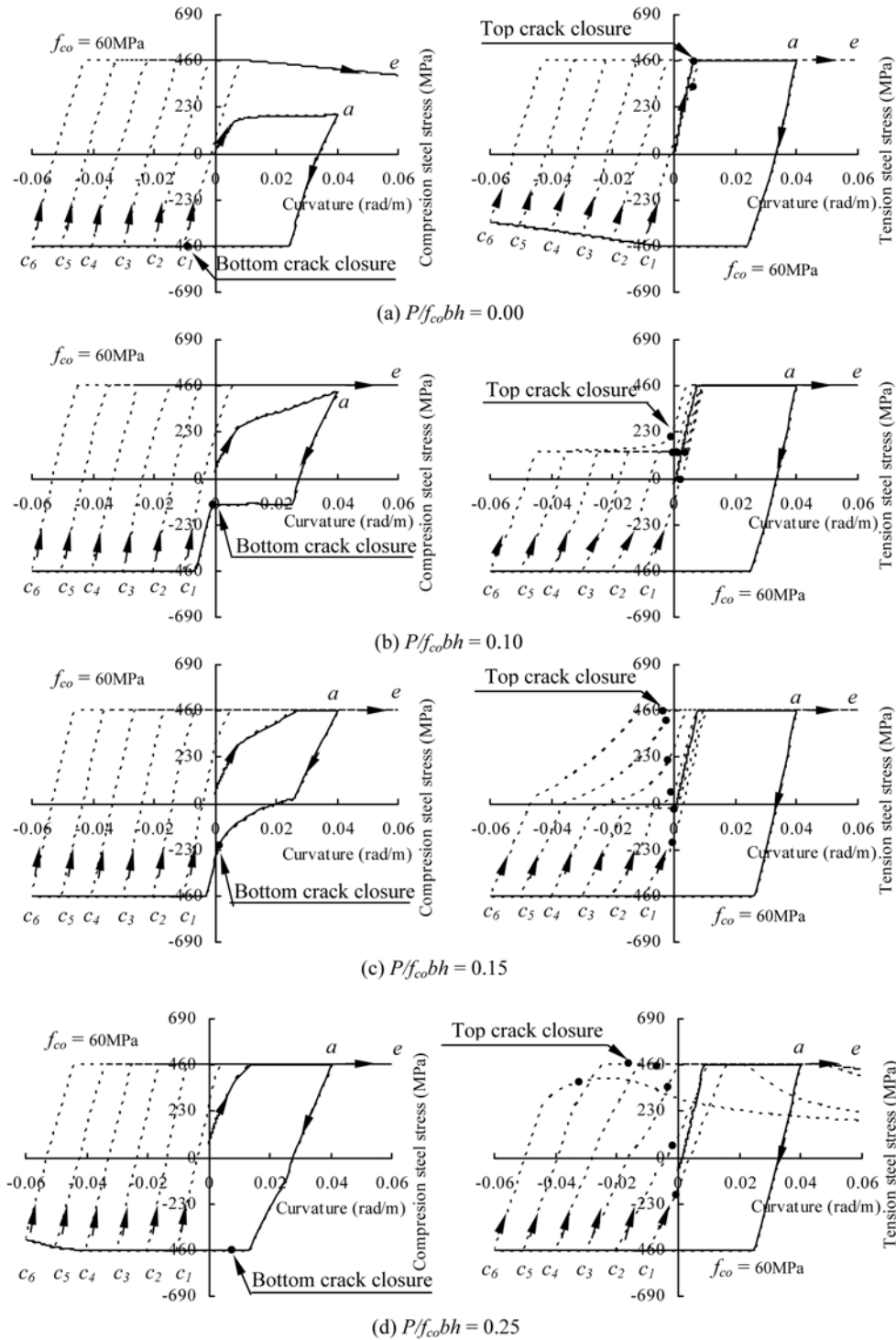
Fig. 14 Variation of steel stress of section under cyclic loading (*in situ* concrete strength = 60 MPa; $\rho_c = \rho_t$ = 2%)

high axial loading, the behaviour after unloading from sagging curvature tends to approach the moment-curvature curve under monotonic loading of hogging moment.

In the second half-cycle, the curvature is increased to a certain sagging curvature at point a and then reversed to a hogging curvature at point c (i.e. c_1, c_2, c_3, c_4, c_5 or c_6). The curvature is again reversed to a large sagging curvature at point e. Two values of curvature at point a are studied, and the results are plotted in Figs. 12 and 13 for sections with *in situ* concrete strength 30 and 90 MPa. In general, the curves in the second half-cycle have characteristics similar to those of the first half-cycle. For cases of low axial loading (e.g. Figs. 12(a)-(e) and 13(a)-(e)), the curves of reloading merge at a point with fairly low sagging curvature. Then further reloading follows a common path returning to the moment-curvature curve of monotonic loading in sagging moment at a point close to the reversal point a in the first half-cycle. For cases of very high axial load (e.g. Figs. 12(f) and 13(f)), some moment-curvature curves in the second half-cycle reach peak sagging moment at hogging curvature, and neither merging appears nor is the moment-curvature curve under monotonic loading in sagging moment ever followed again.

To explain the above phenomena, the variations of stresses and neutral axis depth are further studied. The steel stresses of a section with *in situ* concrete strength 60 MPa and steel ratios $\rho_c = \rho_t = 2\%$ under reversed cyclic loading are plotted in Fig. 14. In general, reversed cyclic loading induces tensile and compressive stresses in the steel reinforcement alternately. In the first half-cycle, the tension reinforcement always yields in tension while the compression reinforcement only yields at sufficiently high axial load level. Around the end of the first half-cycle when the bottom crack closes, there can be a sharp increase in tensile stress in compression reinforcement if it has not yielded yet in order to balance the resulting concrete compression near the bottom. In the first phase of the second half-cycle, the compression reinforcement normally yields in tension and remains yielded for cases of relatively low axial loading while it may unload after yielding for cases of high axial loading. The tension reinforcement normally yields in compression but minor stress reversal is observed at low axial load level. No sharp increase in stress in tension reinforcement is observed when the bottom crack closes, but in some cases of low axial load level the closure of top crack after one cycle is accompanied by a sharp increase in stress to balance the resulting concrete compression near the top. In general, the behaviour of reinforcement under cyclic loading is significantly affected by the axial load level.

The variation of neutral axis depth d_n for sections undergoing reversed cyclic loading is rather complex but it helps to explain some of the phenomena observed. Regardless of the sign of curvature, d_n denotes the distance of neutral axis below the top concrete fibre. If the strain of the section is entirely compressive or tensile, the theoretical neutral axis is obtained from extrapolation as the location where the strain is zero. Therefore points in the first and second quadrants indicate that the section strains are entirely tensile and compressive respectively. For the special case of zero curvature, the neutral axis depth d_n will be undefined. When the curvature changes sign, the neutral axis depth d_n normally alternates between positive and negative infinity. The variation of neutral axis depth d_n for a section with *in situ* concrete strength 60 MPa and steel ratios $\rho_c = \rho_t = 2\%$ under reversed cyclic loading is plotted in Fig. 15. In particular, the phase of loading after the first full cycle is shown in dash line and it normally approaches the curve for monotonic loading in sagging moment from the beginning. The movement of the neutral axis depends very much on the axial load level, and two different typical modes are identified. The neutral axis in a section under low axial loading as shown in Fig. 15(a) continues to rise throughout the first half-cycle as the compression steel remains elastic in the first phase of the half-cycle while it yields extensively in

(a) $P/f_{co}bh = 0.10$ (b) $P/f_{co}bh = 0.25$
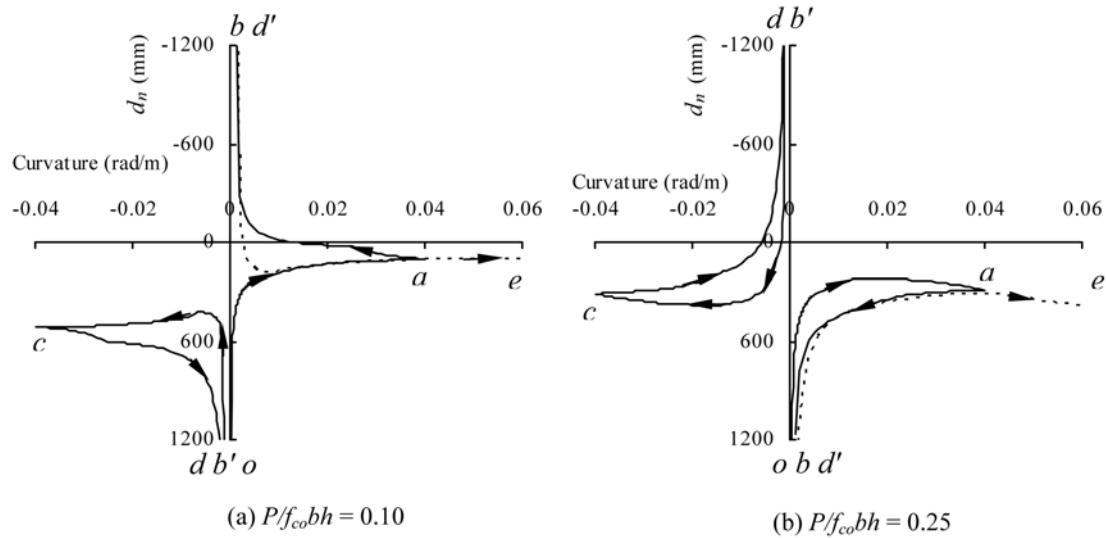
Fig. 15 Variation of neutral axis depth of section under cyclic loading (*in situ* concrete strength = 60 MPa; $\rho_c = \rho_t = 2\%$)

the second phase whereas the tension steel yields extensively in the first phase but unloads shortly after entering into the second phase. One complete cycle therefore creates a net permanent tensile strain in the section as the transition between points d and d' is from the third quadrant to the first quadrant. The behaviour of a section under high axial loading as shown in Fig. 15(b) is typical of less ductile behaviour. In the first phase of the first half-cycle, the neutral axis rises to a high point and then drops gradually leading to reduction in lever arm and hence resisting moment. The neutral axis continues to drop in the second phase. A net permanent compressive strain is created in the section by the complete cycle as the transition between points d and d' is from the second quadrant to the fourth quadrant. The net permanent strains created in the section under different axial load levels by the complete cycle of maximum imposed curvature of 0.04 rad/m are summarized in Table 1. In general, a section under low axial loading tends to elongate because of largely alternating plastic deformation of top and bottom steel. However a section under high axial loading tends to shorten mainly because of the gradual softening of concrete due to cyclic loading.

To further understand the roles of various stresses in the cyclic behaviour of column sections under different axial load levels, the variations of stresses in the initial three quarters of the first cycle of a section with *in situ* concrete strength 30 MPa and steel ratios $\rho_c = \rho_t = 1\%$ under reversed cyclic loading are studied. Fig. 16 shows the variation of steel stresses and moment while Fig. 17

Table 1 Permanent axial strains caused by one complete cycle of flexural deformation (*in situ* concrete strength = 60 MPa; $\rho_c = \rho_t = 2\%$; maximum imposed curvature = 0.04 rad/m)

| $P/f_{co}bh$	Permanent strain
0.00	-4791×10^{-6}
0.10	-1483×10^{-6}
0.15	28×10^{-6}
0.25	1349×10^{-6}
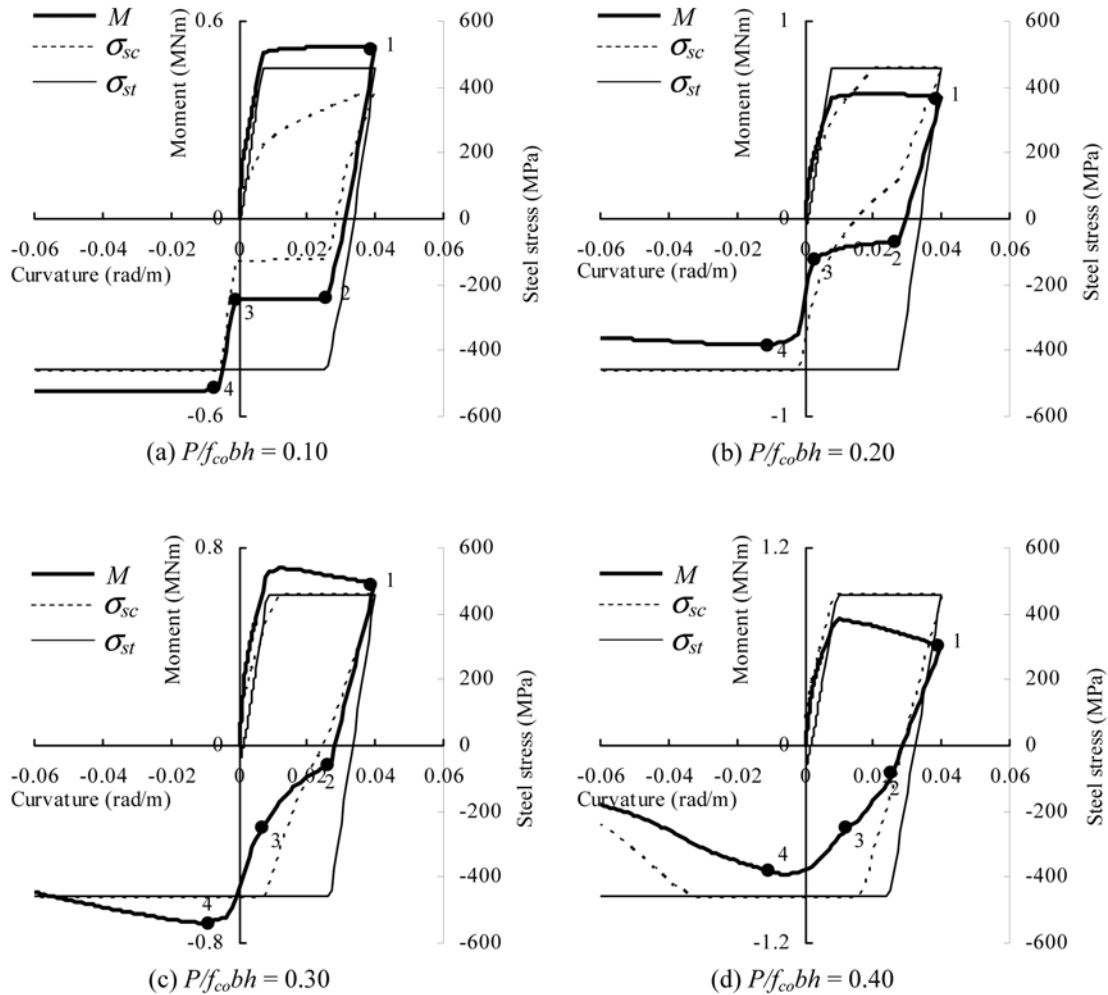
Fig. 16 Variation of steel stresses and moment of section under cyclic loading (*in situ* concrete strength = 30 MPa; $\rho_c = \rho_t = 1\%$)

shows some of the corresponding unconfined concrete stresses. To visualize the effects of various stresses, four typical points are marked. Point 1 denotes the state when reversal just starts from the maximum sagging curvature. Point 2 corresponds to the state when tension steel just yields in compression. Point 3 corresponds to the closure of bottom crack. Point 4 is the state when an arbitrary hogging curvature of -0.01rad/m is reached. During the reversal from points 1 to 2, a straight moment-curvature path is followed in Fig. 16 irrespective of the axial load level, which is largely in parallel with similar trends in the steel stresses. Further reversal from points 2 to 3 is accompanied by an increase in hogging moment except for the case of very low axial load level. Actually for the case of $P/f_{co}bh = 0.10$, Fig. 17(a) shows that the neutral axis keeps rising during the first half-cycle and little compression is taken by concrete at point 2 after almost total unloading of concrete in compression. During the reversal from points 2 to 3, the tension steel remains yielded in compression while the stress in compression steel has to keep fairly constant to satisfy axial
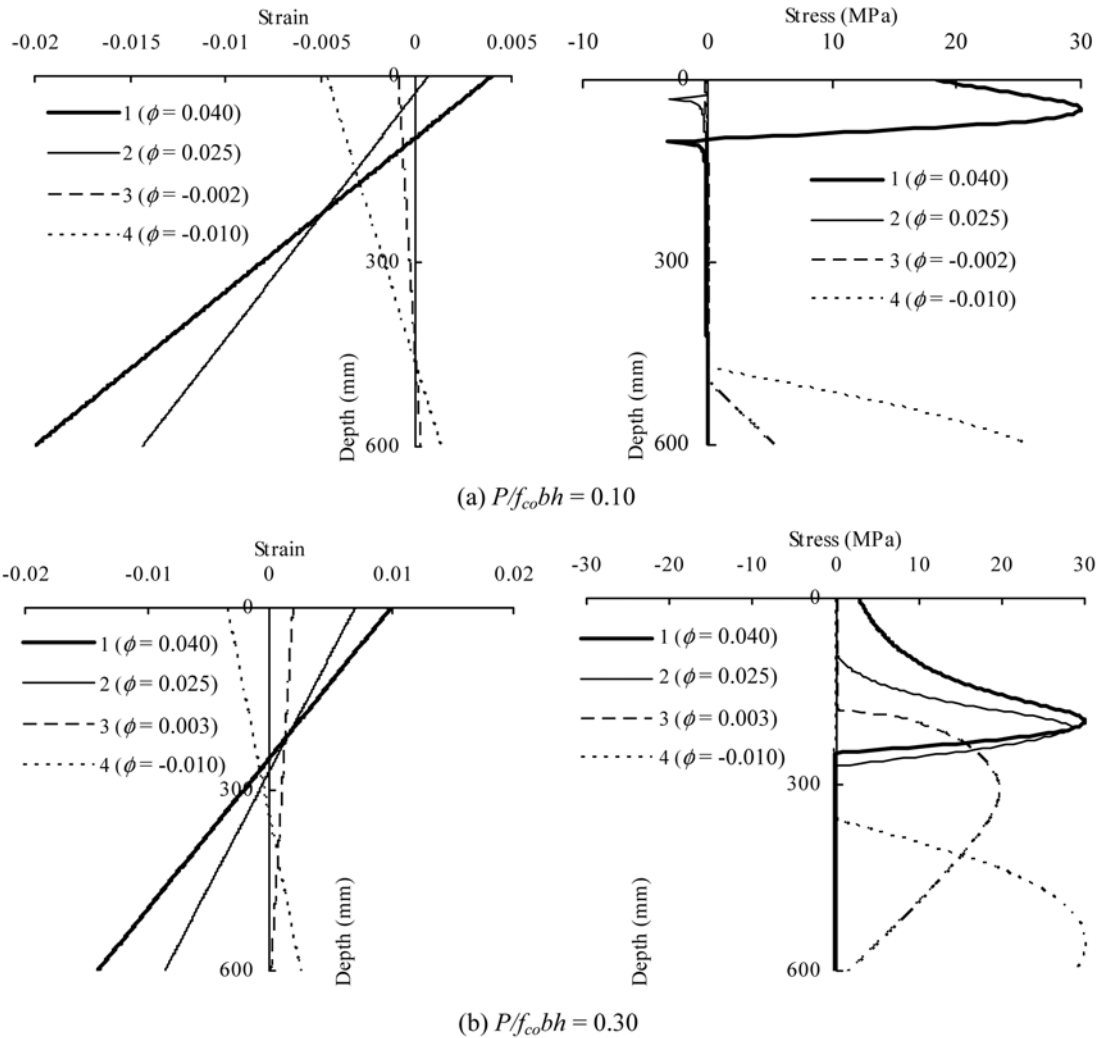
Fig. 17 Variation of strain and concrete stress of section under cyclic loading (*in situ* concrete strength = 30 MPa; $\rho_c = \rho_t = 1\%$)

equilibrium. Therefore the resisting moment remains almost constant until the closure of bottom crack (i.e. point 3). The additional concrete compression that results from bottom crack closure stiffens the section and increases the resisting hogging moment between points 3 and 4. The behaviour of the section under higher axial load level (e.g. $P/f_{co}bh = 0.30$) is much different. Fig. 17(b) shows that during reversal from points 1 to 3, the neutral axis drops continuously while the concrete compression remains pivotal.

6. Conclusions

The full-range cyclic flexural behaviour of symmetrical RC columns cast of normal- and high-

strength concrete is studied using a numerical method that employs the actual stress-strain curves of the constitutive materials and takes into account the stress-path dependence of concrete and steel reinforcement. Particular attention is paid to the post-peak stage. The study confirms that the axial load level governs the full-range behaviour of RC columns under both monotonic and cyclic loading. The following conclusions are drawn.

• The moment capacity under monotonic loading tends to increase with compressive axial load level up to around $P/f_{co}bh$ = 0.4 or 0.5, beyond which the moment capacity drops. However with increasing axial load, the flexural ductility factor always decreases.

• Except for very low axial load levels, the compression reinforcement yields under monotonic loading and remains yielded. In most cases, the tension reinforcement yields with strain reversal and unloading at the post-peak stage. In the absence of axial loading or at very low axial loading, the tension reinforcement yields but does not unload. Under sufficiently high compressive axial loading, the tension reinforcement does not yield at all.

• The full-range moment-curvature curve under monotonic loading of a section under relatively low axial loading is characterized by a long plateau around peak moment, while that under relatively high axial loading has a sharper peak. Moreover, the full-range moment-curvature curves for monotonic loading give the envelope for cyclic response, except for sections under very high axial loading.

• At relatively low axial load level, the neutral axis of an RC column section under monotonic loading keeps rising with curvature. For medium to high axial load level, the neutral axis rises first but drops again beyond a certain curvature at the post-peak stage giving rise to strain reversal at the tension steel.

• The sequential opening and closure of cracks of an RC column section under cyclic loading do affect its stiffness and general behaviour.

• The movement of the neutral axis of an RC column section under cyclic loading depends very much on the axial load level, and two different typical modes are identified. The net permanent axial strains caused in RC column sections undergoing cyclic flexural deformation depend on the axial load levels. In general, a section under low axial loading tends to elongate because of largely alternating plastic deformation of top and bottom steel. However a section under high axial loading tends to shorten mainly because of the gradual softening of concrete due to cyclic loading.

References

ACI Committee 363 (1992), *State-of-the-art report on high strength concrete*, ACI 363-R92, American Concrete Institute, Detroit, U.S.A.

Attard, M. M. and Setunge, S. (1996), "The stress-strain relationship of confined and unconfined concrete", *ACI Mater. J.*, **93**(5), 432-442.

Attard, M. M. and Stewart, M. G. (1998), "A two parameter stress block for high-strength concrete", *ACI Struct. J.*, **95**(3), 305-317.

Au, F. T. K., Bai, B. Z. Z., and Kwan, A. K. H. (2005), "Complete moment-curvature relationship of reinforced normal- and high-strength concrete beams experiencing complex load history", *Comput. Conc., An Int. J.*, **2**(4), 309-324.

Au, F. T. K. and Kwan, A. K. H. (2004), "A minimum ductility design method for non-rectangular high-strength concrete beams", *Comput. Conc., An Int. J.*, **1**(2), 115-130.

Azizinamini, A., Corley, W. G., and Johal, L. S. P. (1992), "Effects of transverse reinforcement on seismic

performance of columns", *ACI Struct. J.*, **89**(4), 442-450.

Azizinamini, A., Kuska, S. S. B., Brungardt, P., and Hatfield, E. (1994), "Seismic behavior of square high-strength concrete columns", *ACI Struct. J.*, **91**(3), 336-345.

Bai, Z. Z., Au, F. T. K., and Kwan, A. K. H., "Complete nonlinear response of reinforced concrete beams under cyclic loading", *The Structural Design of Tall and Special Building* (to appear).

Carreira, D. J. and Chu, K. H. (1986), "The moment-curvature relationship of reinforced concrete members". *ACI J.*, **83**(2), 191-198.

Elmorsi, M., Kianoush, M. R., and Tso, W. K. (1998), "Nonlinear analysis of cyclically loaded reinforced concrete structures", *ACI Struct. J.*, **95**(6), 725-739.

Gerald, C. F. and Wheatley, P. O. (1999), *Applied Numerical Analysis*, 6th Ed., Addison-Wesley, USA, 698pp.

Guo, Z. H. and Zhang, X. Q. (1987), "Investigation of complete stress-deformation curves for concrete in tension", *ACI Mater. J.*, **84**(4), 278-285.

Ho, J. C. M. and Pam, H. J. (2003), "Inelastic design of low-axially loaded high-strength reinforced concrete columns", *Eng. Struct.*, **25**(8), 1083-1096.

Hwang, S. K. and Yun, H. D. (2004), "Effects of transverse reinforcement on flexural behavior of high-strength concrete columns", *Eng. Struct.*, **26**(1), 1-12.

Kwan, A. K. H. and Au, F. T. K. (2004), "Flexural strength-ductility performance of flanged beam sections cast of high-strength concrete", *The Structural Design of Tall Buildings*, **13**(1), 29-43.

Kwan, A. K. H., Au, F. T. K., and Chau S. L. (2004), "Effects of confinement on flexural strength and ductility design of HS concrete beams", *The Structural Engineer*, **8**(23-24), 38-44.

Menegotto, M. and Pinto, P. E. (1973), "Method of analysis for cyclically loaded reinforced concrete plane frames including changes in geometry and non-elastic behavior of elements under combined normal force and bending". *IABSE Symposium, Resistance and Ultimate Deformability of Structures Acted on by Well-Defined Repeated Loads, Lisbon, Spain*.

Pam, H. J., Kwan, A. K. H. and Ho, J. C. M. (2001), "Post-peak behavior and flexural ductility of doubly reinforced normal- and high-strength concrete beams", *Struct. Eng. Mech.*, **12**(5), 459-474.

Sakai, K. and Sheikh, S. A. (1989), "What do we know about confinement in reinforced concrete columns? (A critical review of previous work and code provisions)", *ACI Struct. J.*, **86**(2), 192-207.

Sheikh, S. A. and Yeh, C. C. (1990), "Tied concrete columns under axial load and flexure", *J. Struct. Eng.*, **116**(10), 2780-2800.

Soroushian, P., Sim, J., and Hsu, J. W. (1991), "Axial/flexural behavior of reinforced concrete sections. Effects of the design variable", *ACI Struct. J.*, **88**(1), 17-21.

Notation

A_{sc} = area of top reinforcement

A_{st} = area of bottom reinforcement

b = breadth of rectangle beam section

d_1 = depth to centroid of top reinforcement

d = depth to centroid of bottom reinforcement

h = total depth of the beam section

d_n = neutral axis depth measured on the section with zero axial strain

d_g = depth to section geometric centre

E_c = Young's modulus of concrete

E_s = Young's modulus of steel reinforcement

f_i = stress at inflection point on descending branch of stress-strain curve of concrete

f_{co} = *in situ* uniaxial compressive strength of concrete

f_r = confining stress

f_o = confined compressive strength of concrete
f_t = tensile strength of concrete
f_y = yield strength of steel reinforcement
x = depth from top fibre
ε_c = strain in concrete
ε_{ce} = compressive strain at extreme compression fibre of concrete
ε_i = strain at inflection point on descending branch of stress-strain curve of concrete
ε_o = strain in concrete at peak stress
ε_{pc} = residual plastic strain in concrete
ε_{ps} = residual plastic strain in steel reinforcement
ε_s = strain in steel reinforcement
ε_{sc} = compressive strain in compression reinforcement
ε_{st} = tensile strain in tension reinforcement
ε_t = tensile strain at tensile strength of concrete
ρ_c = compression steel ratio (= A_{sc}/bd)
ρ_t = tension steel ratio (= A_{st}/bd)
σ_c = stress in concrete
σ_s = stress in steel reinforcement
ϕ = curvature of section

CC